

# Predictable and Unpredictable Components of Cape Town Winter Rainfall

BENJAMIN A. CASH<sup>a,b</sup>, NATALIE J. BURLS<sup>a,b</sup>, AND LAILA V. HOWAR<sup>c</sup>

<sup>a</sup> Department of Atmospheric, Oceanic, and Earth Sciences, George Mason University, Fairfax, Virginia

<sup>b</sup> Center for Ocean–Land–Atmosphere Studies, George Mason University, Fairfax, Virginia

<sup>c</sup> Department of Atmospheric and Oceanic Science, University of Maryland, College Park, Maryland

(Manuscript received 8 August 2022, in final form 6 February 2023, accepted 11 April 2023)

**ABSTRACT:** In early 2018, due in part to a severe and extended meteorological drought, Cape Town was at risk of being one of the first major metropolitan areas in the world to run out of water. The magnitude of the crisis was exacerbated by the fact that such a prolonged and severe drought was both unanticipated and unpredicted. In this work, we analyze data from both observations and seasonal forecasts made as part of the North American Multimodel Ensemble (NMME) to better understand the predictability of rainfall in the Cape Town (CT) region. We find that there are statistically significant correlations between observed CT rainfall and sea surface temperatures in the tropical Atlantic ( $\sim 0.45$ ) as well as a pattern of 200-mb geopotential height (z200) anomalies resembling the Southern Annular Mode (SAM;  $\sim 0.4$ ). Examination of hindcasts from the NMME demonstrates that the models accurately reproduce the observed correlation between CT rainfall and z200 anomalies. However, they fail to reproduce correlations between CT rainfall and the tropical South Atlantic. Decomposition of the correlations into contributions from predictable and unpredictable components indicates that CT rainfall in the models is dominated by unpredicted atmospheric variability (correlation  $\sim 0.84$ ) relative to predicted (correlation  $\sim 0.14$ ), which may be related to the failure to simulate the connection with the tropical Atlantic.

**SIGNIFICANCE STATEMENT:** Water crises are occurring with increasing severity and frequency around the globe. The ability to accurately forecast wet season rainfall would be invaluable to water managers and other decision-makers. Here, we explore the reasons behind the failure of a suite of operational seasonal forecast models to accurately predict rainfall in the Cape Town region of South Africa.

**KEYWORDS:** Africa; Coupled models; Model evaluation/performance; Interannual variability; Seasonal forecasting


## 1. Introduction

The city of Cape Town (population  $\sim 3.7$  million) is situated in the Western Cape region of South Africa. Cape Town (CT) receives most of its rainfall during the months of April–September and is relatively dry the rest of the year. In early 2018, due in part to a severe and extended meteorological drought, Cape Town was at risk of being one of the first major metropolitan areas in the world to run out of water. The magnitude of the crisis was exacerbated by the fact that such a prolonged and severe drought was both unanticipated and unpredicted (Joubert and Ziervogel 2019).

CT rainfall exhibits considerable interannual variability, as well as a tendency toward prolonged dry periods, and is supplied primarily by cold fronts associated with extratropical cyclones and occasional cut-off lows. These systems bring rainfall onto land as part of the climatological northward shift of the Southern Ocean storm track during austral winter (Reason and Rouault 2005; Blamey and Reason 2007). The interannual variability of CT rainfall is associated with a number of slowly varying climate features that might be expected to provide enhanced predictability on seasonal time scales,

such as sea surface temperatures (SSTs) in the South Atlantic (Reason et al. 2002; Reason and Jagadheesha 2005), sea ice anomalies in the Atlantic sector of the Southern Ocean (Blamey and Reason 2007), El Niño–Southern Oscillation (ENSO; Ropelewski and Halpert 1987; Reason et al. 2002; Mulenga et al. 2003; Colberg et al. 2004; Rouault et al. 2010; Philippon et al. 2012), and the Southern Annular Mode (SAM; Reason et al. 2002; Philippon et al. 2012; Mahlalela et al. 2019), as well as Hadley cell expansion and storm-track displacement (Sousa et al. 2018; Burls et al. 2019).

Previous research has shown that CT austral winter rainfall is positively correlated with ENSO, a source of potential predictability on seasonal time scales. This correlation may arise through a variety of potential links. Previous studies have shown rainfall variability in the CT is influenced by SST gradients in the South Atlantic and south Indian basins, the variability of which has been linked to ENSO (Colberg et al. 2004; Philippon et al. 2012). The systems that bring rain to the region are also deeper, larger, and located farther north during El Niño, whereas these systems are thinner, smaller, and located farther south during La Niña (Philippon et al. 2012). Rouault et al. (2010) found a negative correlation between CT rainfall anomalies and SST anomalies in the South Atlantic that could be linked to wind speed changes during ENSO events. The atmospheric dynamic fields during the time of wet spells over this region feature lower pressure and northwesterly wind anomalies during El Niño, as well as higher pressure and southerly wind anomalies during La Niña (Philippon et al. 2012).

 Denotes content that is immediately available upon publication as open access.

Corresponding author: Benjamin A. Cash, bcash@gmu.edu

DOI: 10.1175/JCLI-D-22-0593.1

© 2023 American Meteorological Society. This published article is licensed under the terms of the default AMS reuse license. For information regarding reuse of this content and general copyright information, consult the AMS Copyright Policy ([www.ametsoc.org/PUBSReuseLicenses](http://www.ametsoc.org/PUBSReuseLicenses)).

Other proposed mechanisms through which El Niño events give rise to dry winters include alterations in the local Walker circulation and SST in the tropical Indian and Atlantic Oceans. During an El Niño event, the convergence zone of cloud bands that are usually the source of high CT rainfall moves offshore (Tyson and Preston-Whyte 2000). The south Indian convergence zone (SICZ) flow moves northeastward and prevails over the Indian Ocean, causing dry conditions over South Africa (Mulenga et al. 2003; Blamey and Reason 2012).

In addition to ENSO, the SAM has also been shown to have a large influence on tropospheric circulation variability in the Southern Hemisphere (Hartmann and Lo 1998; Thompson and Wallace 2000; Reason and Rouault 2005; Abram et al. 2014). The positive phase of the SAM has been shown to favor dry conditions over Cape Town, while the negative phase favors wet conditions. The importance of understanding relationships between the SAM and the regional winter climate is underscored by the recent shift in the SAM toward a more positive phase, which has contributed to the observed long-term southward shift of the midlatitude westerlies and drier winters over much of the Southern Hemisphere (Seager et al. 2003, 2019; Fogt and Bromwich 2006; Pohl et al. 2010; L'Heureux and Thompson 2006).

The systematic change in the rainfall associated with cold fronts appears to be linked to the expansion of the Hadley cell across the Southern Hemisphere and an increasing trend in postfrontal high pressure conditions that suppress orographically enhanced rainfall (Burls et al. 2019). The circulation has expanded the most poleward during summer and fall in both hemispheres (Grise et al. 2018). Observational evidence shows that the expanding Hadley circulation pushes subtropical dry regions farther poleward in both hemispheres, enacting dry spells (Seidel et al. 2008; Davis and Rosenlof 2012; Birner et al. 2014; Lucas et al. 2014).

In this work, we further explore and understand the predictability of rainfall in the CT region by analyzing the individual models and ensemble members available from the North American Multimodel Ensemble (NMME; Kirtman et al. 2014). We find that, while the NMME can reproduce the patterns of rainfall and 200-mb height anomalies associated with CT rainfall variability, those patterns are dominated by unpredicted variability. We also find that the models fail to reproduce observed correlations between CT rainfall and tropical South Atlantic SSTs, which may be a contributing factor in the lack of predictability.

## 2. Data and methodology

### a. Data

We analyze a subset of the NMME hindcasts initialized 1 March and integrated through September of that same year at a minimum and whose output data of predicted SST, precipitation, and 200-mb geopotential height (z200) have been made available through the International Research Institute data library (see Table 1) for the April–September (AMJJAS) 1982–2009 hindcast period.

In addition to the NMME, we analyze data from the CPC Merged Analysis of Precipitation (CMAP; Xie and Arkin 1997),

the Extended Reconstructed Sea Surface Temperature, version 4 (ERSST.v4), product (Huang et al. 2015), 200-mb geopotential height data from the Modern-Era Retrospective Analysis for Research and Applications, version 2 (MERRA-2), product (Gelaro et al. 2017), and a station-based precipitation time series for the CT reservoir catchment basin (see Burls et al. 2019).

### b. Methodology

Our analysis follows the approach described in Cash and Burls (2019) in leveraging the large number of individual ensemble members in the NMME to assess the relative importance of predicted and unpredicted climate variations in CT rainfall. For each model and ensemble member, we decompose model fields into two components, for example,

$$\text{SST}_{ij}^A = \text{SST}_{ij}^E + \text{SST}_{ij}^N, \quad (1)$$

where  $\text{SST}_{ij}^A$  is the total SST field (minus the grand mean such that the average over all seasons and members is 0 for season  $i$  and ensemble member  $j$ ),  $\text{SST}_{ij}^E$  is the ensemble mean for season  $i$ , and  $\text{SST}_{ij}^N$  is the deviation of a given ensemble member  $j$  for a given season  $i$  from the ensemble mean. In the case where the ensemble mean is calculated for a single model,  $\text{SST}_{ij}^E$  is the component of SST that is common to all ensemble members and thus is relatively insensitive to small changes in initial conditions. In the case where the ensemble mean is calculated over multiple models [multimodel ensemble mean (MMEM)], it is also the component that is not overly sensitive to differences in model formulation.

Following the nomenclature used in Cash and Burls (2019), we refer to  $\text{SST}_{ij}^E$  as the predicted or forced component.  $\text{SST}_{ij}^N$  in turn represents the component of the simulated field that is sensitive to initial conditions and/or model formulation and is referred to as the unpredicted component (or sometimes simply noise). Note that both the predicted and unpredicted components are defined for each model (or collection of models) and variable separately and are thus explicitly both model and variable dependent.

Using this decomposition, we can assess the contribution from the different components to the total correlation. For example, the Pearson's correlation between SST and CT rainfall can be written as

$$\rho_A = \frac{\sum(\text{SST}^E + \text{SST}^N)(\text{CT}^E + \text{CT}^N)}{\sqrt{\sum(\text{SST}^A)^2} \sqrt{\sum(\text{CT}^A)^2}}, \quad (2)$$

which can be further rewritten as

$$\rho_A = \frac{\sum(\text{SST}^E \text{CT}^E + \text{SST}^N \text{CT}^N)}{\sqrt{\sum(\text{SST}^A)^2} \sqrt{\sum(\text{CT}^A)^2}} \approx \frac{\sum \text{SST}^E \text{CT}^E}{\sqrt{\sum(\text{SST}^A)^2} \sqrt{\sum(\text{CT}^A)^2}} + \frac{\sum \text{SST}^N \text{CT}^N}{\sqrt{\sum(\text{SST}^A)^2} \sqrt{\sum(\text{CT}^A)^2}}. \quad (3)$$

Here, we have dropped the ensemble/noise cross terms as their contribution to the total is negligible. The first term on the right-hand side of Eq. (3), denoted here as  $\rho_{AE}$ , represents

TABLE 1. NMME models included in this study. Most acronym expansions are available at <http://www.ametsoc.org/PubsAcronymList>. Other expansions include Forecast-Oriented Low Ocean Resolution Model using parameter set B (FLORB), Forecast-Oriented Low Ocean Resolution Model using parameter set A (FLORA), Canadian Meteorological Centre (CMC), CCCma's fourth-generation ocean model, level 40 (CanOM4L40), Rosenstiel School of Marine and Atmospheric Sciences (RSMAS), and Parallel Ocean Program (POP), level 42 (POPL42).

Model	Hindcast Period	Ensemble size	Forecast lead (months)	Native atmosphere resolution	Native ocean resolution	Reference
NCEP-CFSv2	1982–2010	24	0–9	TI26L64	MOM4L40, 0.25°/28 km Eq	Saha et al. (2014)
GFDL-CM2p5 FLORB01	1982–2010	12	0–11	CI8L32 (50 km)	MOM4L50, 0.3°/33 km Eq	Vecchi et al. (2014)
GFDL-CM2p5 FLORA06	1982–2010	12	0–11	CI8L32 (50 km)	MOM4L50, 0.3°/33 km Eq	Vecchi et al. (2014)
CMC1-CanCM3	1982–2010	10	0–11	T63L31	CanOM4L40, 0.94°/104 km Eq	Merryfield et al. (2013)
CMC2-CanCM4	1982–2010	10	0–11	T63L315	CanOM4L40, 0.94°/104 km Eq	Merryfield et al. (2013)
NCAR-CCSM3 (COLA-RSMAS)	1982–2010	6	0–11	T85L26	POPL42, 0.3°/33 km Eq	Kirtman and Min (2009)
NCAR-CCSM4 (COLA-RSMAS)	1982–2010	10	0–11	0.9° × 1.25°, L26	POPL60, 0.25°/28 km Eq	Infanti and Kirtman (2017)
NASA-GMAO-062012	1982–2010	11	0–11	1° × 1.25°, L72	MOM4L40, 0.25°/28 km Eq	Vernieres et al. (2012)

the contribution to the total  $\rho_A$  from the ensemble-mean terms  $E$  (hence,  $AE$ ), while the second term, denoted  $\rho_{AN}$ , is the contribution from the noise terms  $N$  (hence,  $AN$ ). Note that the denominator of each term is the same and depends on the variance of  $SST^A$  and  $CT^A$ .

We can also calculate the correlation of the ensemble mean or noise terms separately, for example,

$$\rho_E = \frac{\sum SST^E CT^E}{\sqrt{\sum (SST^E)^2} \sqrt{\sum (CT^E)^2}},$$

$$\rho_N = \frac{\sum SST^N CT^N}{\sqrt{\sum (SST^N)^2} \sqrt{\sum (CT^N)^2}}. \quad (4)$$

These correlations emphasize the relationships between features within the ensemble mean and noise, respectively, as opposed to the contribution of the ensemble mean and noise to the total. It is important to note that  $\rho_{AE} \neq \rho_E$ ,  $\rho_{AN} \neq \rho_N$ , and

$\rho_A \neq \rho_E + \rho_N$ , due to the differences in the denominators. The impact of this change in the denominator can be substantial (see Figs. 2e,f and associated discussion below).

All reported correlations are tested for statistical significance using a two-tailed  $t$  test at the 95% confidence level. Since significance is a function of the degrees of freedom, and the total data used to calculate each correlation coefficient vary with the component considered, the numerical value for significance varies widely across calculations. The observational period chosen consists of 28 years of data (1982–2009), corresponding to the hindcast period of the NMME. In contrast, the NMME subset analyzed consists of the same 28-yr subset, but also includes eight models with a total of 95 ensemble members for a total of 2660 years. Analysis of the model ensemble means results in one 28-yr time series per model for a total of 224 years. For 28 years, magnitudes above 0.375 are significant at the 95% level using a two-tailed  $t$  test. For 224 years, magnitudes above 0.13 are significant at the 95% level. For

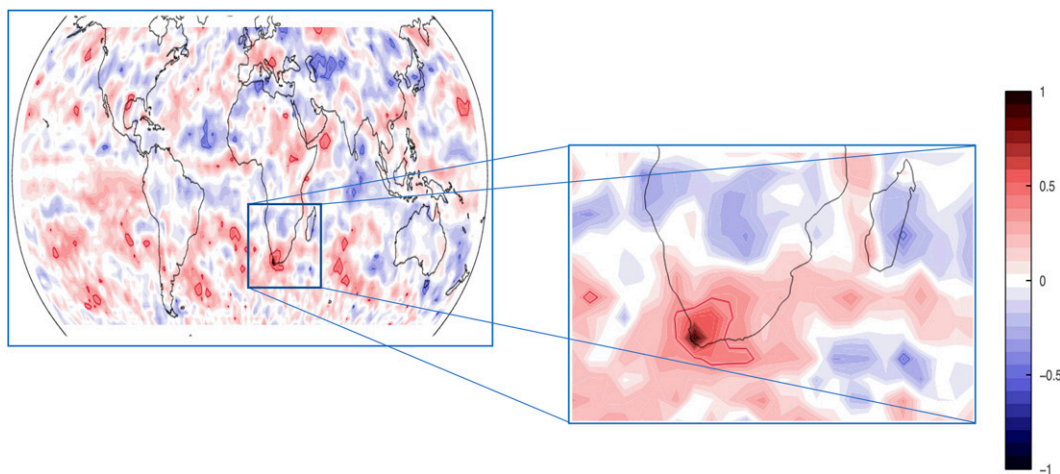


FIG. 1. One-point correlation map of CMAP CT rainfall index with global CMAP rainfall for 1982–2009 during AMJJAS. Values with magnitudes above 0.375 are significant at the 95% level as determined by a two-tailed  $t$  test.



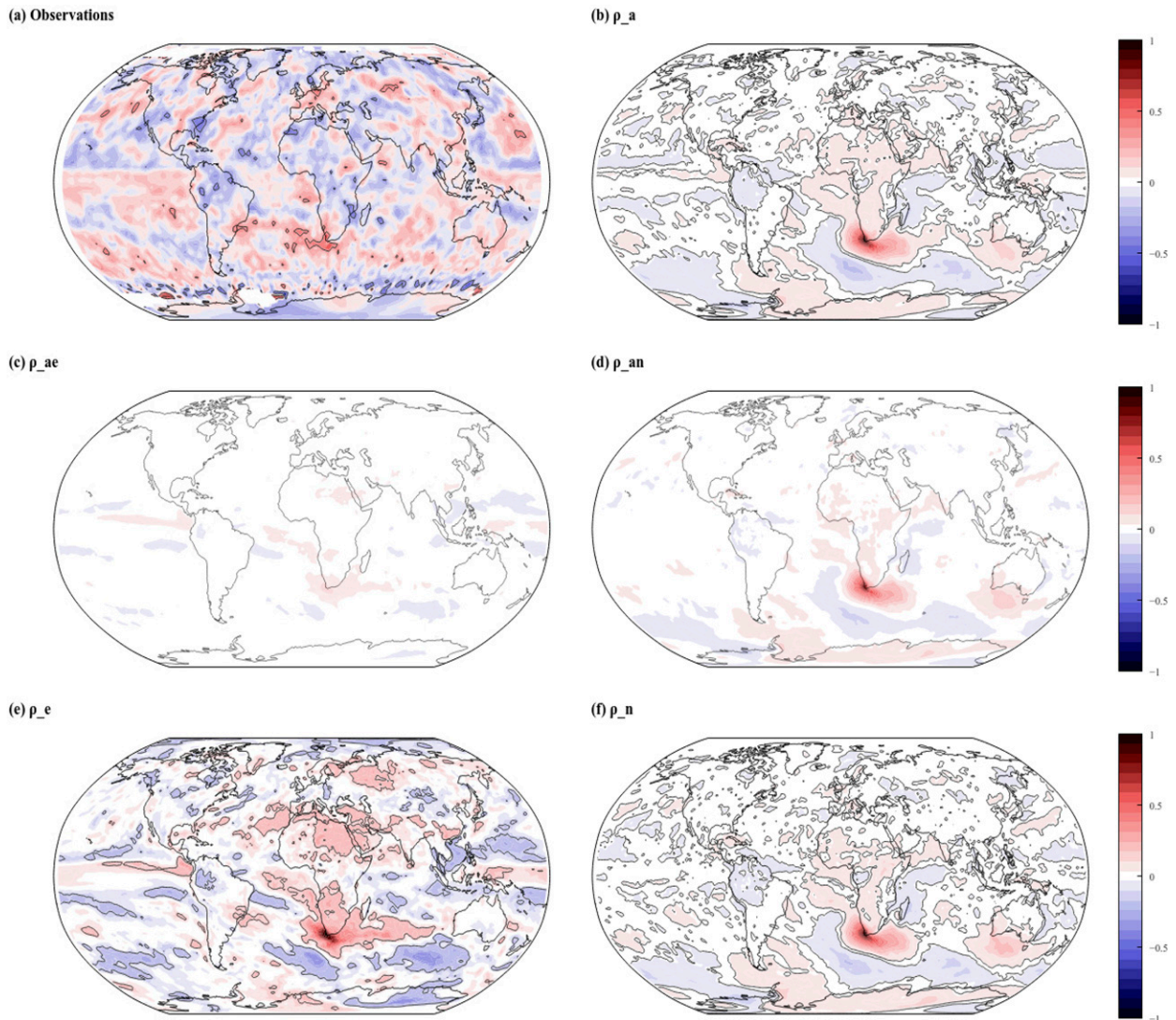


FIG. 2. One-point correlation map decomposition for CT rainfall index and global rainfall for 1982–2009 during AMJJAS. (a) Observed correlation for CT station index (Burls et al. 2019) and CMAP global rainfall. (b) Total correlation ( $\rho_a$ ) for NMME model in Table 1. (c) Contribution of ensemble mean ( $\rho_{AE}$ ) to total correlation  $\rho_a$ . (d) Contribution of noise component ( $\rho_{AN}$ ) to total correlation  $\rho_a$ . (e) One-point correlation map for ensemble-mean precipitation only. (f) One-point correlation map for noise component rainfall only.

2660 years, any value displayed is statistically significantly different from zero, if not necessarily physically significant.

### 3. Results

We first consider the patterns of rainfall associated with Cape Town rainfall variability by constructing a rainfall index centered on the Western Cape region (defined as  $35^{\circ}$ – $33^{\circ}$ S,  $18^{\circ}$ – $20^{\circ}$ E) using the CMAP data and correlating it with rainfall at every other point in the CMAP dataset. Correlations are relatively high in the immediate vicinity of Cape Town (see Fig. 1 inset) by construction, with lower values distributed noisily across the globe and generally below the 95% confidence level outside of the region surrounding Cape Town. As previous work has shown that results can be quite

sensitive to the choice of observed rainfall product (Cash et al. 2015), we repeat the global correlation map calculation using a composite Cape Town station rainfall time series (see Burls et al. 2019) in place of the CMAP time series. When we recalculate the one-point correlation pattern (Fig. 2a), we find that the maximum correlation values of the Cape Town station data and CMAP are only 0.52 in the immediate vicinity of Cape Town. Given the relatively coarse resolution of the CMAP gridded data ( $2.5^{\circ} \times 2.5^{\circ}$ ) and the sharp geographic variations in rainfall characteristics in the Western Cape region (Landman et al. 2001), the station time series from Burls et al. (2019) is used to represent CT rainfall for the remainder of this work.

Compared to the observed correlation pattern, the noisiness of the total model correlation pattern ( $\rho_a$ ; Fig. 2b) between

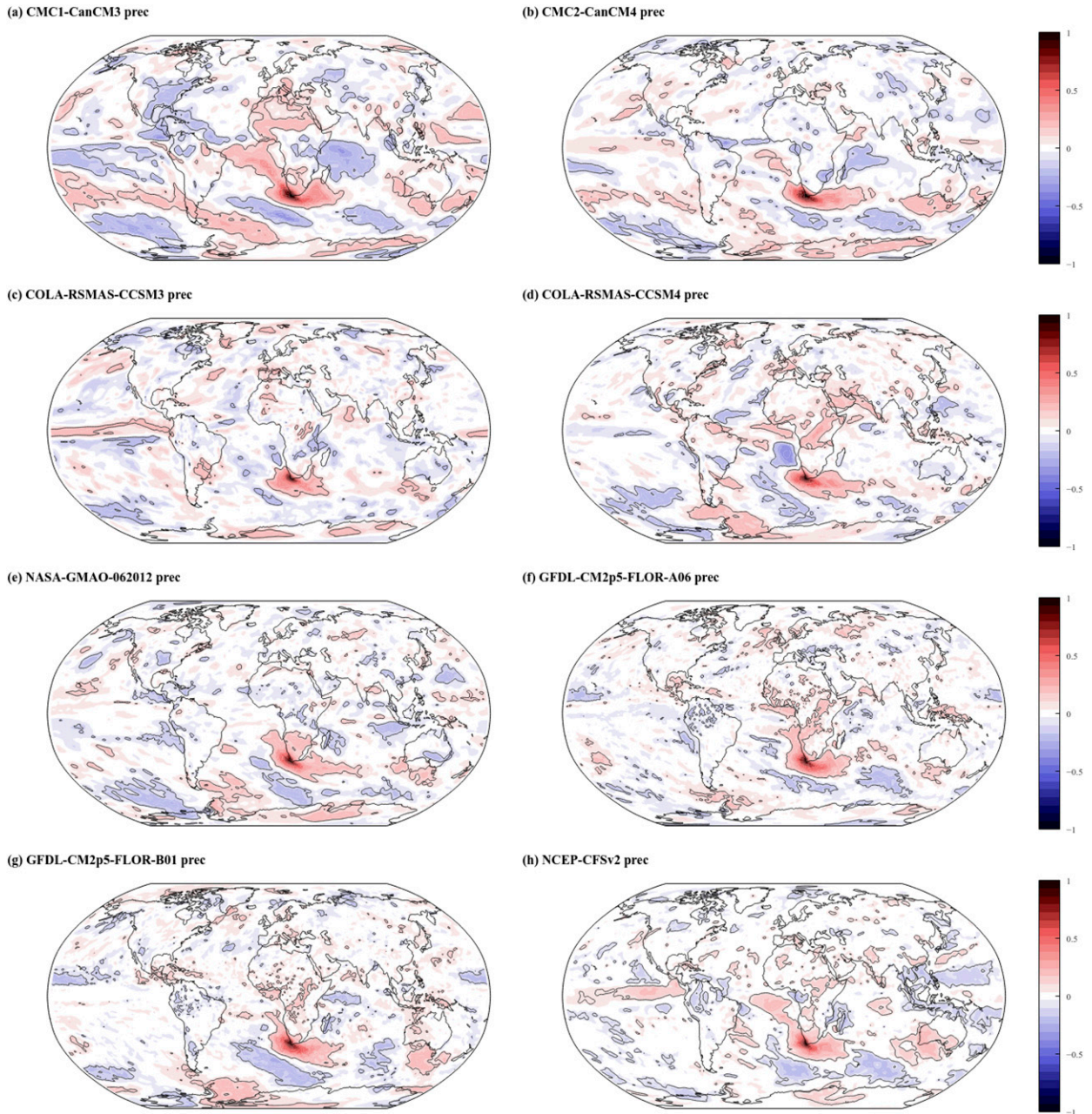


FIG. 3. Total correlation ( $\rho_a$ ) CT and global rainfall for individual models in Table 1. See panel title for individual model plotted. The precise value significant at the 95% level varies with the number of ensemble members, but in general, values above 0.15 can be considered significant.

simulated Cape Town index rainfall variability and rainfall at every other point is significantly reduced and includes only relatively weak centers of action outside of the CT region. Recalling that 95 times more data are used in Fig. 2b than in Fig. 2a, the reduction in noisiness is an expected result. Further decomposing the model correlation ( $\rho_{AE}$ ;  $\rho_{AN}$ ; Fig. 2d) shows that almost all of the overall correlation pattern (Fig. 2b) is due to the noise component. This is consistent with previous work showing that the prediction skill of winter season rainfall is generally low over

the CT region (Landman et al. 2001), as well as the specific observation that the day zero drought was not well anticipated (Joubert and Ziervogel 2019).

Analyzing the ensemble mean ( $\rho_E$ ) in isolation presents a very different picture of the role of the predictable component (cf. Figs. 2c,e). The reduced variance in the denominator [see Eq. (3)] leads to much higher magnitudes overall for  $\rho_E$  relative to  $\rho_{AE}$ . The noise-only component ( $\rho_N$ ; Fig. 2f) is relatively unchanged from Fig. 2d, reflecting its dominant



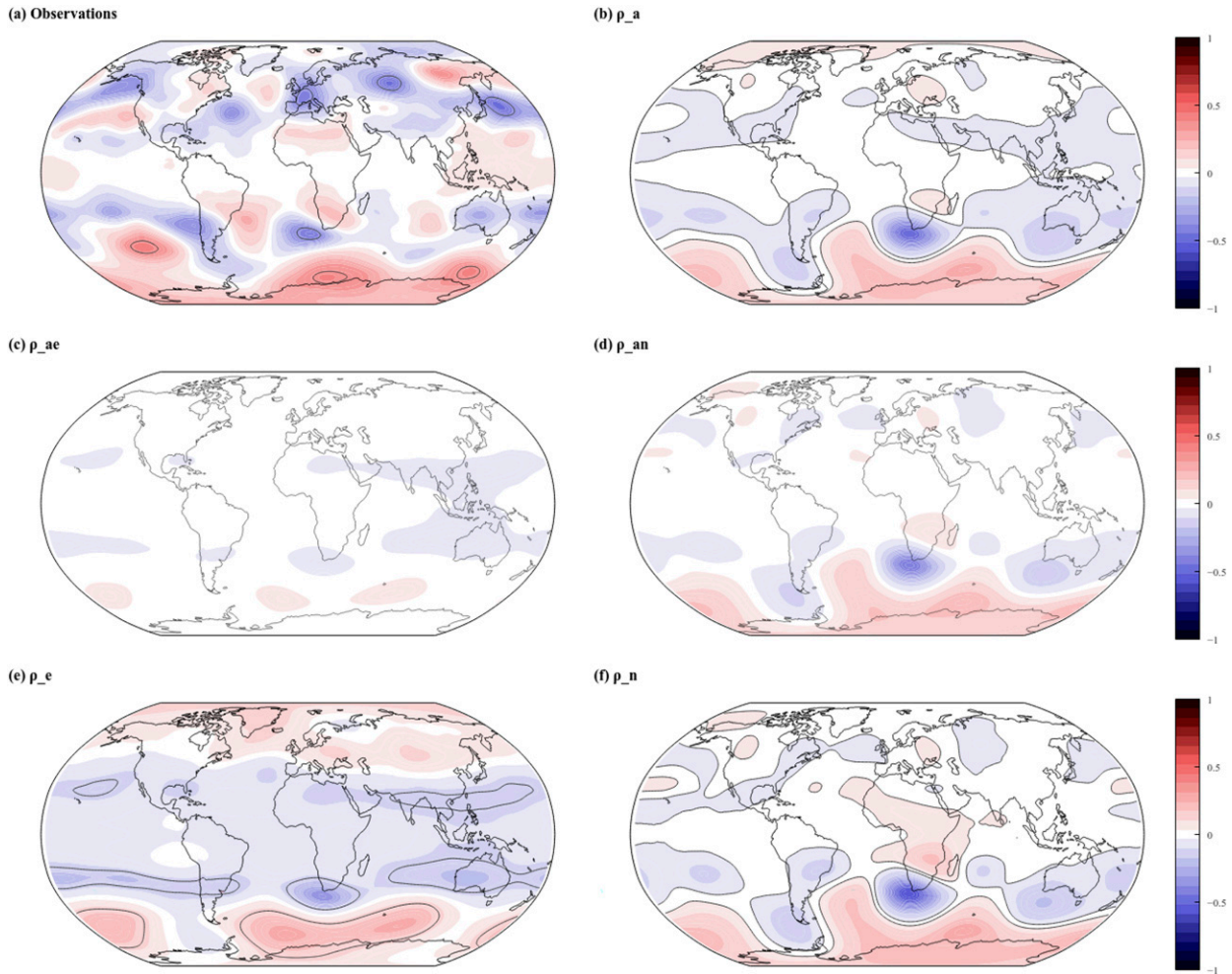


FIG. 4. As in Fig. 2, but for correlations between CT rainfall and 200-mb heights.

contribution to  $\rho_A$ . Analyzing the ensemble-mean component in isolation thus acts to exaggerate its influence (e.g., Cash and Burls 2019), although it also has been argued that this is necessary to counter the tendency of climate models to produce too much internal variability and overemphasize the role of noise (e.g., Scaife and Smith 2018). It is thus important to note that Fig. 2 does not necessarily mean that CT rainfall is unpredictable in nature, merely that variability in the selected NMME models is dominated by unpredicted variations.

In addition to the differences between observations and simulation, Figs. 2a and 2b include vastly different amounts of data, due to the use of multiple models and multiple ensemble members in Fig. 2b. To assess the impact of the increased data available to the MME, as well as potential sensitivities to model formulation, we also calculate the point correlation between global and CT rainfall separately for each model (Fig. 3). By construction, each model shows the same high positive correlation in the CT region as the observations (Fig. 2a) and MME (Fig. 2b). However, the correlations now show a much greater magnitude outside of the CT region, with significant intermodel variability. For example, depending on

the model chosen, it is possible to find statistically significant swaths of positive (Fig. 3c) or negative (Fig. 3a) correlation with the tropical Pacific. These differences arise despite each panel still including data from multiple ensemble members. The observed correlation patterns in Fig. 2a, along with the individual model patterns in Fig. 3, should thus all be interpreted with a certain amount of caution and an awareness of the impacts of sampling variability.

Based on previous analyses of CT rainfall variability (e.g., Reason et al. 2002), we expect to find a strong association with local circulation anomalies. Correlating observed CT rainfall and z200 (Fig. 4a), we find a pattern that closely resembles the negative phase of the SAM. Increased CT rainfall is associated with positive z200 anomalies over Antarctica and a zonally elongated region of negative anomalies across the midlatitudes, including a center of strong negative correlations located SW of the CT region. It is worth noting the association with centers near Chile and Australia, regions that have also experienced severe drought in recent decades.

We find that the observed correlations between CT rainfall and z200 are reasonably well reproduced in the NMME (see

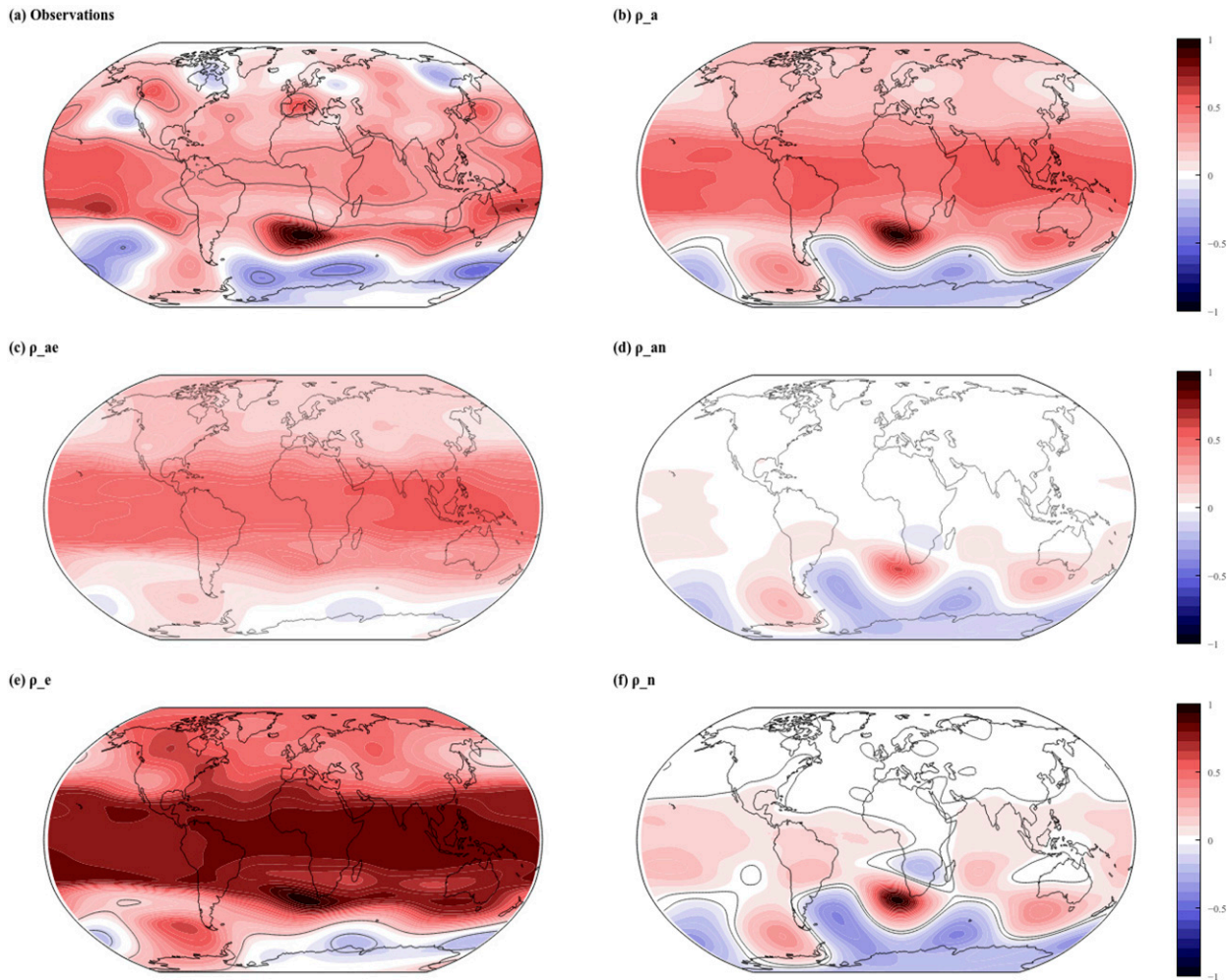


FIG. 5. Correlation decomposition for 200-mb height index centered southwest of the CT region and global 200-mb height field. Panels are as in Figs. 2 and 4. Note the close similarity between (a) and (b).

Fig. 4b). The region of observed positive correlations over the Antarctic (Fig. 4a) is clearly identifiable, as are the negative correlations stretching across the Pacific from Australia to South America. As with the local rainfall correlation patterns, the model 200-mb height pattern is dominated by the noise component (cf. Figs. 4c,d). Thus, while the models accurately represent the link between z200 and rainfall, they are unable to predict the relevant 200-mb height anomalies on seasonal time scales. Analyzing the predictable component in isolation (Fig. 4e) shows that it is associated with a tropics-wide decrease in 200-mb heights and a stronger center of negative correlations to the immediate south of Cape Town.

Given the apparent impact of z200 variability on CT rainfall, particularly the center to the immediate southwest of the Cape Town region, we repeat the correlation analysis described above using a z200 index (defined as 39°–34°S, 6°–11°E) that characterizes that center in place of the CT rainfall. Correlating this index with z200 globally, in the observations (Fig. 5a), we see the expected strong, positive correlations in the region that defines the index. We also find positive

correlations across the tropics, indicating that positive z200 anomalies in the CT region are, at least in part, associated with an increase in heights across the tropics. Such an increase would be consistent with an association with El Niño conditions and previous research showing dry conditions (recall that CT rainfall is negatively correlated with the z200 center) typically occur in Cape Town during El Niño events. We also recover the expected (now negative) correlations over the Antarctic region associated with the SAM signal.

Comparing the model total z200 correlation pattern (Fig. 5b) to the observations (Fig. 5a), we find they are remarkably similar, even down to the center of positive correlations off the southern tip of South America. In contrast to the analysis of z200 and rainfall (Fig. 4), here we find a significant contribution from the predictable component of the simulations (cf. Figs. 5d,b). The predictable component is associated with positive correlations across the entirety of the tropics, resembling a combination consistent with the summer response to the positive phase of ENSO (see Kumar and Hoerling 2003) and with previous work demonstrating that the



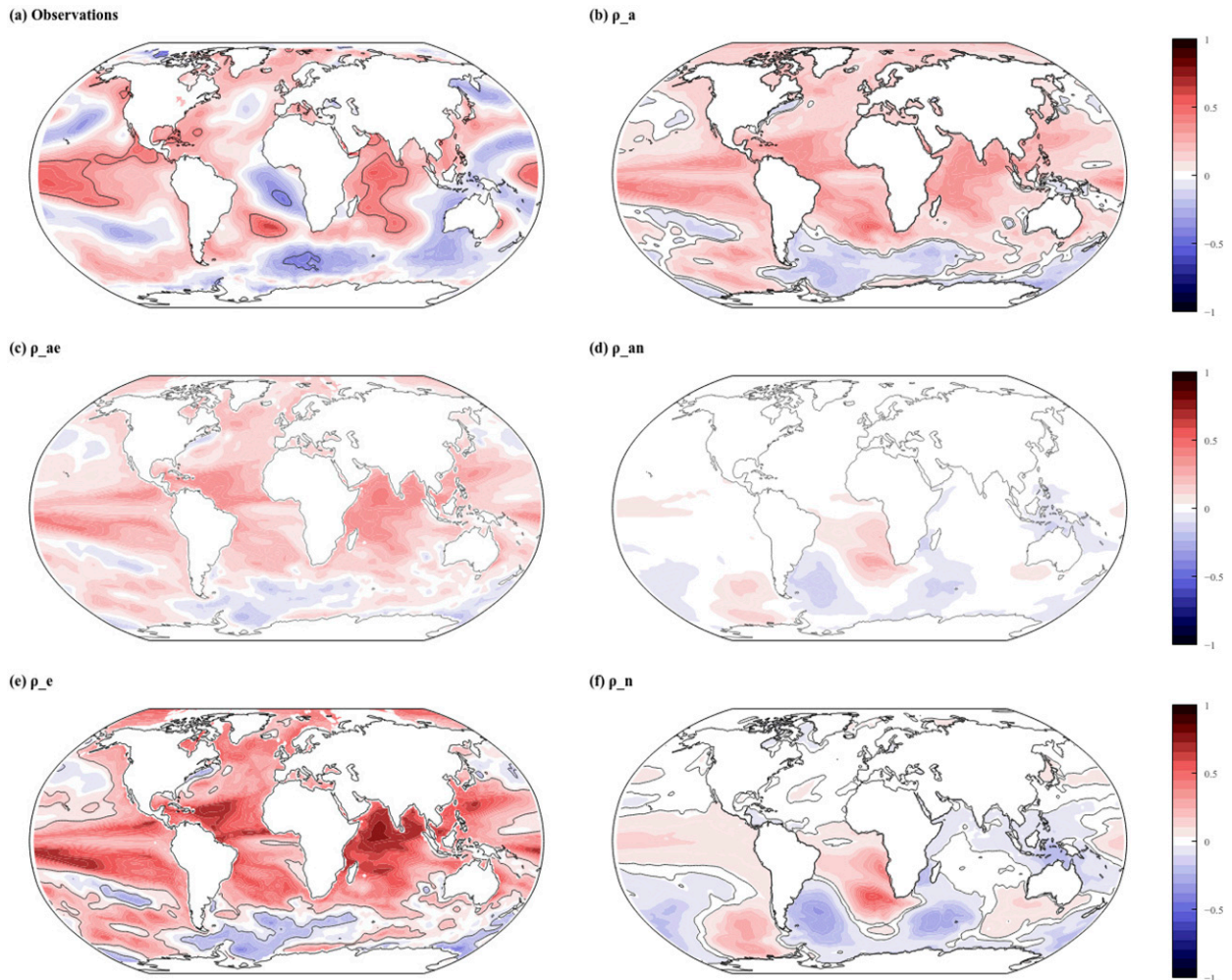


FIG. 6. As in Fig. 5, but for correlation between z200 index and SST. Panels are as in Figs. 2, 4, and 5. Note the discrepancy between (a) and (b) in the South Atlantic.

predictable component of the NMME is dominated by the ENSO response (Cash and Burls 2019). The noise component (Fig. 5e) is more locally confined and contributes most of the amplitude over the pole. Interestingly, the center near the southern tip of South America and the critical center southwest of Cape Town are both superpositions of predictable and unpredictable components of the simulation.

We further investigate the potential contributors to the predictable component of the z200 anomaly, including the implied link to ENSO, by calculating the correlation decomposition for our 200-mb height index and SST (Fig. 6). The observations (Fig. 6a) show a pattern of positive correlations across the tropical Pacific that resemble the decaying positive phase of ENSO [e.g., see Kumar and Hoerling (2003), Fig. 5], consistent with Fig. 5a. We also find positive correlations in the western Indian Ocean, and negative correlations across the eastern Indian Ocean, a pattern that closely resembles the Indian Ocean dipole mode (Saji et al. 1999) and much of the South Atlantic. Most notably, while the model pattern resembles the observations in the eastern tropical Pacific and the

Southern Ocean, the regions of negative correlation in the South Atlantic and eastern Indian Ocean are absent in the simulations.

In contrast to the correlation between CT rainfall and 200-mb heights, we find that the global z200–SST correlation pattern (Fig. 6b) is dominated by the predictable component (Fig. 6c). The noise component (Fig. 6d) consists mostly of a center in the tropical South Atlantic that is opposite in sign to the observations (cf. Fig. 6a). The absence of the strong negative correlation between the 200-mb height index and the South Atlantic is common to all models examined in this work (see Fig. 7). The negative correlation with the eastern Indian Ocean is also generally absent, although not as completely (see Fig. 7d).

Finally, we return to analysis of the direct association between CT rainfall and SST (Fig. 8). In contrast to the correlation between CT precipitation and global precipitation (Fig. 2), but consistent with the association between the z200 center and SST (Figs. 6 and 7), the association between CT rainfall and SST differs significantly between the models



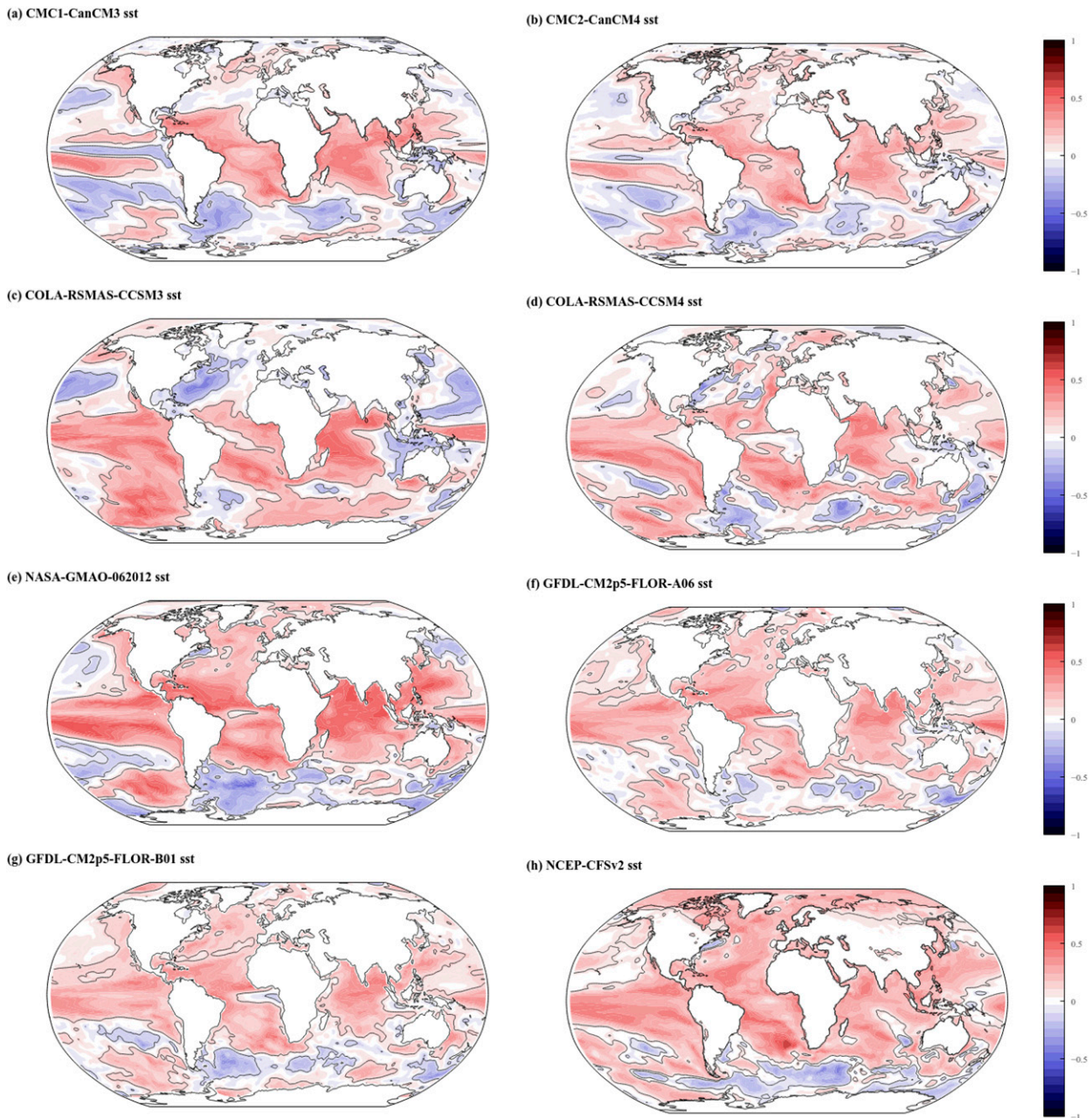


FIG. 7. Correlation between z200 index and SST for individual models.

and observations (cf. Figs. 8a,b). Model correlations in the South Atlantic are weaker than observed and are also opposite in sign (Figs. 8a,b). The total correlation is dominated by the noise term (cf. Figs. 8c,d), consistent with the dominant role of noise in the precipitation patterns (see Fig. 2). Correlations with the tropical Pacific are drastically reduced relative to Fig. 6, although there is a similar pattern when the predictable component is considered in isolation (Fig. 8e). Similarly, the observed South Atlantic pattern can be seen when the predictable component is considered in isolation (Fig. 8e). However, the magnitudes in the Atlantic

are small and not statistically significant such that the noise signal dominates over all (Fig. 8b).

Further exploring the relationship between CT rainfall and the remote ocean basins, we find that the observed winter correlation shows a region of positive correlation of  $\sim 0.5$  in the South Atlantic (Fig. 8a). This is broadly consistent with previous analyses of the relationship between CT region rainfall and the South Atlantic (Blamey and Reason 2007). The Blamey and Reason (2007) analysis used different datasets, analysis periods, and methodologies to arrive at a similar result, indicating this is a relatively robust relationship. We also

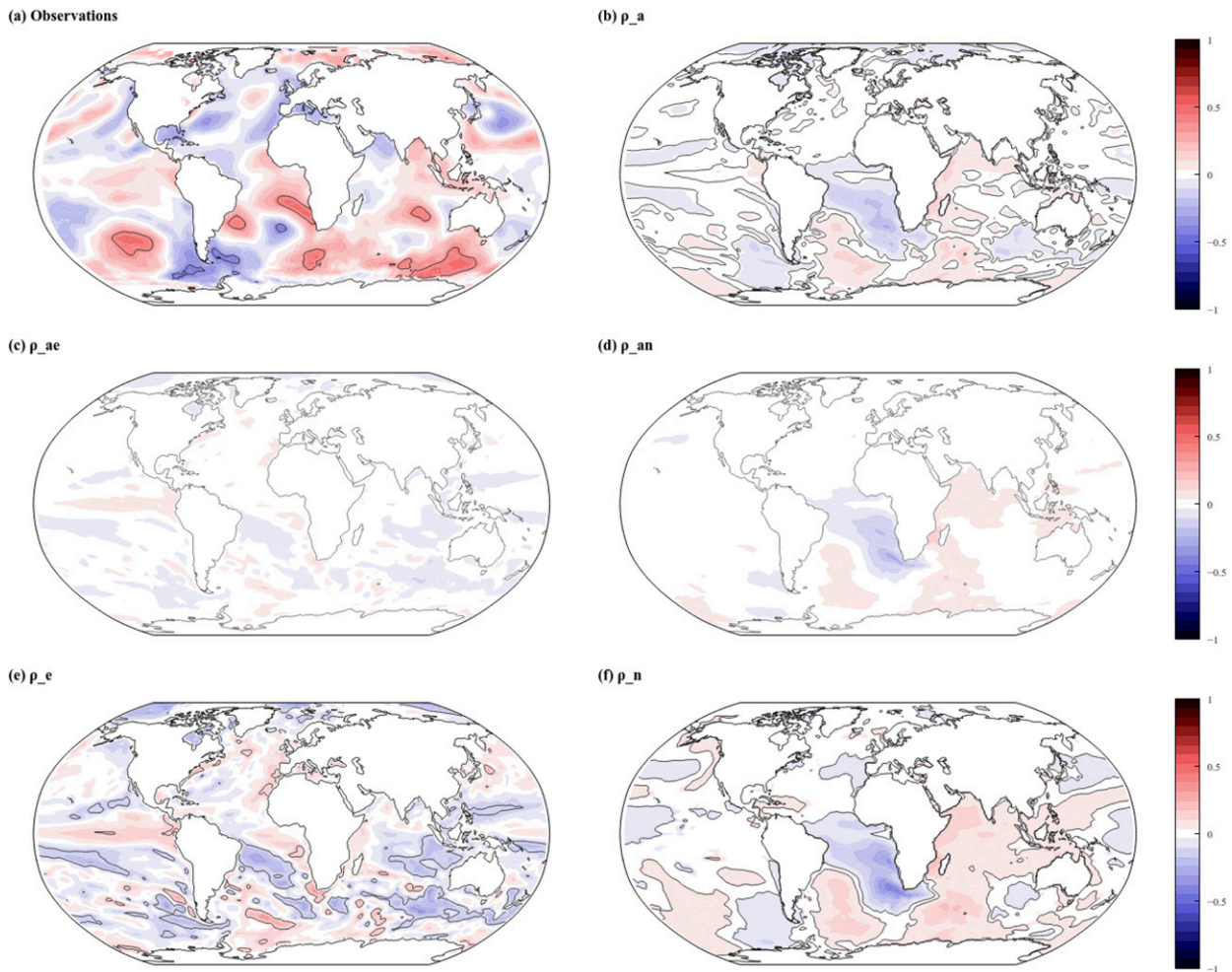


FIG. 8. As in Figs. 2, 4, 5, and 6, but for correlation between CT rainfall and SST.

find a positive correlation with the eastern tropical Pacific in the observations, although the values are not significantly different from zero.

#### 4. Summary and conclusions

Accurate predictions of seasonal rainfall are both a scientific Grand Challenge<sup>1</sup> and of tremendous practical importance. The severity of the Cape Town “day zero” water crisis was in part attributable to the fact that it was both unanticipated and unpredicted (Joubert and Ziervogel 2019). In this work, we analyze the variability and predictability of Cape Town winter rainfall in both models and observations. Consistent with the previous studies discussed in the introduction, we find that variations in Cape Town winter rainfall are associated with changes in circulation across the globe. Our results show that increased winter rainfall is associated with increases in local rainfall and with SST in the South Atlantic, eastern

Pacific, and western Indian Oceans. We also find associations with negative SST anomalies in the eastern Indian Ocean, as well as with the negative phase of the Southern Annular Mode. The fact that rainfall variations are associated with these global-scale patterns of variability raises the possibility that Cape Town winter rainfall is potentially more predictable than the current state of the art would suggest.

In addition to the observations, in this work we also analyze data from a subset of dynamical models from the NMME. We find that the models are able to reproduce some, but not all, of the observed relationships. In particular, the correlation between Cape Town and global rainfall, as well as Cape Town rainfall 200-mb heights, closely matches what is observed, but the observed correlations between rainfall and SST are not well captured. This discrepancy is particularly notable in the South Atlantic, where the observed correlations are positive, and the model correlations are negative. This indicates that, while the models are correctly identifying the state of the atmosphere that results in increased rainfall, they are failing to correctly link that atmospheric state and global SST. This hypothesis is further supported by decomposing the model

<sup>1</sup> [https://www.noaa.gov/sites/default/files/2022-01/PPGC-Strategy\\_FINAL\\_2020-1030.pdf](https://www.noaa.gov/sites/default/files/2022-01/PPGC-Strategy_FINAL_2020-1030.pdf).



correlations into predictable and unpredictable components, which shows that the unpredictable components dominate the model correlations in almost all cases. Thus, even in the case of the high-fidelity reproduction of the observed 200-mb height relationship with rainfall, we find the models have little skill in predicting its occurrence on seasonal time scales.

One possible explanation for this domination by the noise component is simply that Cape Town rainfall is driven by chaotic atmospheric variability on seasonal time scales and is fundamentally unpredictable. However, it should also be noted that our previous work (Burls et al. 2019) has shown that the recent trend in rainfall days in the Cape Town region is associated with a decrease in the number of rainy days associated with the passage of winter cold fronts. Given the relatively coarse resolution of the models in the NMME, and their focus on seasonal predictability, it is likely that these much smaller-scale interactions are not represented well. In addition, the complex and abrupt changes in topography of the Western Cape cannot be captured at NMME resolutions. The use of high-resolution, convection-allowing or convection-permitting models thus might improve the representation of seasonal Western Cape (WC) rainfall. However, at this point, the computational cost of such models remains prohibitive for large seasonal ensembles and thus any potential improvement remains speculative.

The fact that the models fail to capture the much larger-scale relationship between Cape Town rainfall and global SST suggests that SST biases, particularly in the Atlantic, may be preventing models from realizing the potential predictability associated with these more slowly varying components of the climate system. Coupled climate models suffer from significant biases in the tropical and subtropical South Atlantic [see Counillon et al. (2021) and references therein]. Previous analyses (e.g., Gimeno et al. 2012) have shown that this region of the Atlantic and the nearby regions of the Southern Ocean are the primary source of winter moisture for the Cape Town region (see their Fig. 11). It is thus entirely consistent with these previous studies that systematic errors in South Atlantic SST should lead to systematic errors in WC rainfall. That this is, in fact, a systemic issue in the models is further demonstrated by the fact that none of the eight models analyzed in this work are able to reproduce the observed associations with Atlantic SST. The fact that the models do not recover the observed global relationships between Cape Town rainfall and Atlantic SST suggests that reducing or eliminating these biases represents a potential mechanism for improving seasonal predictions of Cape Town rainfall.

*Acknowledgments.* This research is supported by grants from the National Science Foundation (NSF) (AGS-1613318, AGS-1338427, AGS-1740693), the National Oceanic and Atmospheric Administration (NOAA) (NA14OAR4310160), and NASA (NNX14AM19G). We acknowledge the agencies that support the NMME-Phase II system, and we thank the climate modeling groups (Environment Canada, NASA, NCAR, NOAA/GFDL, NOAA/NCEP, and University of Miami) for producing and making available their model output. NOAA/NCEP,

NOAA/CTB, and NOAA/CPO jointly provided coordinating support and led development of the NMME-Phase II system.

*Data availability statement.* The NMME data used in this study were obtained from the IRI Climate Data Library <http://iridl.ldeo.columbia.edu/SOURCES/Models/NMME/>.

## REFERENCES

- Abram, N. J., R. Mulvaney, F. Vimeux, S. J. Phipps, J. Turner, and M. H. England, 2014: Evolution of the Southern Annular Mode during the past millennium. *Nat. Climate Change*, **4**, 564–569, <https://doi.org/10.1038/nclimate2235>.
- Birner, T., S. M. Davis, and D. J. Seidel, 2014: The changing width of Earth's tropical belt. *Phys. Today*, **67**, 38–44, <https://doi.org/10.1063/PT.3.2620>.
- Blamey, R., and C. J. C. Reason, 2007: Relationships between Antarctic sea-ice and South African winter rainfall. *Climate Res.*, **33**, 183–193, <https://doi.org/10.3354/clr033183>.
- , and —, 2012: Mesoscale convective complexes over southern Africa. *J. Climate*, **25**, 753–766, <https://doi.org/10.1175/JCLI-D-10-05013.1>.
- Burls, N. J., R. C. Blamey, B. A. Cash, E. T. Swenson, A. al-Fahad, M.-J. M. Bopape, D. M. Straus, and C. J. C. Reason, 2019: The Cape Town “day zero” drought and Hadley cell expansion. *npj Climate Atmos. Sci.*, **2**, 27, <https://doi.org/10.1038/s41612-019-0084-6>.
- Cash, B. A., and N. J. Burls, 2019: Predictable and unpredictable aspects of U.S. West Coast rainfall and El Niño: Understanding the 2015/16 event. *J. Climate*, **32**, 2843–2868, <https://doi.org/10.1175/JCLI-D-18-0181.1>.
- , and Coauthors, 2015: Regional structure of the Indian summer monsoon in observations, reanalysis, and simulation. *J. Climate*, **28**, 1824–1841, <https://doi.org/10.1175/JCLI-D-14-00292.1>.
- Colberg, F., C. J. C. Reason, and K. Rodgers, 2004: South Atlantic response to El Niño–Southern Oscillation induced climate variability in an ocean general circulation model. *J. Geophys. Res.*, **109**, C12015, <https://doi.org/10.1029/2004JC002301>.
- Counillon, F., N. Keenlyside, T. Toniazzo, S. Koseki, T. Demissie, I. Bethke, and Y. Wang, 2021: Relating model bias and prediction skill in the equatorial Atlantic. *Climate Dyn.*, **56**, 2617–2630, <https://doi.org/10.1007/s00382-020-05605-8>.
- Davis, S. M., and K. H. Rosenlof, 2012: A multidagnostic inter-comparison of tropical-width time series using reanalyses and satellite observations. *J. Climate*, **25**, 1061–1078, <https://doi.org/10.1175/JCLI-D-11-00127.1>.
- Fogt, R. L., and D. H. Bromwich, 2006: Decadal variability of the ENSO teleconnection to the high-latitude South Pacific governed by coupling with the Southern Annular Mode. *J. Climate*, **19**, 979–997, <https://doi.org/10.1175/JCLI3671.1>.
- Gelaro, R., and Coauthors, 2017: The Modern-Era Retrospective Analysis for Research and Applications, version 2 (MERRA-2). *J. Climate*, **30**, 5419–5454, <https://doi.org/10.1175/JCLI-D-16-0758.1>.
- Gimeno, L., and Coauthors, 2012: Oceanic and terrestrial sources of continental precipitation. *Rev. Geophys.*, **50**, RG4003, <https://doi.org/10.1029/2012RG000389>.
- Grise, K. M., S. M. Davis, P. W. Staten, and O. Adam, 2018: Regional and seasonal characteristics of the recent expansion of the tropics. *J. Climate*, **31**, 6839–6856, <https://doi.org/10.1175/JCLI-D-18-0060.1>.

- Hartmann, D. L., and F. Lo, 1998: Wave-driven zonal flow vacillation in the Southern Hemisphere. *J. Atmos. Sci.*, **55**, 1303–1315, [https://doi.org/10.1175/1520-0469\(1998\)055<1303:WDZFFV>2.0.CO;2](https://doi.org/10.1175/1520-0469(1998)055<1303:WDZFFV>2.0.CO;2).
- Huang, B., and Coauthors, 2015: Extended Reconstructed Sea Surface Temperature version 4 (ERSST.v4). Part I: Upgrades and intercomparisons. *J. Climate*, **28**, 911–930, <https://doi.org/10.1175/JCLI-D-14-00006.1>.
- Infanti, J. M., and B. P. Kirtman, 2017: CGCM and AGCM seasonal climate predictions: A study in CCSM4. *J. Geophys. Res. Atmos.*, **122**, 7416–7432, <https://doi.org/10.1002/2016JD026391>.
- Joubert, L. S., and G. Ziervogel, 2019: Day zero: One city's response to a record-breaking drought. AFC Rep., 31 pp., [https://www.africancentreforcities.net/wp-content/uploads/2019/07/Day\\_Zero\\_Joubert\\_Ziervogel\\_2019.pdf?\\_\\_cf\\_chl=tk=bn7fcwGFGLRYhautUQy999IFGTLEx.O5OmjAyd.CGE-1683086565-0-gaNycGzNC2U](https://www.africancentreforcities.net/wp-content/uploads/2019/07/Day_Zero_Joubert_Ziervogel_2019.pdf?__cf_chl=tk=bn7fcwGFGLRYhautUQy999IFGTLEx.O5OmjAyd.CGE-1683086565-0-gaNycGzNC2U).
- Kirtman, B. P., and D. Min, 2009: Multimodel ensemble ENSO prediction with CCSM and CFS. *Mon. Wea. Rev.*, **137**, 2908–2930, <https://doi.org/10.1175/2009MWR2672.1>.
- , and Coauthors, 2014: The North American Multimodel Ensemble: Phase-1 seasonal-to-interannual prediction; Phase-2 Toward developing intraseasonal prediction. *Bull. Amer. Meteor. Soc.*, **95**, 585–601, <https://doi.org/10.1175/BAMS-D-12-00050.1>.
- Kumar, A., and M. P. Hoerling, 2003: The nature and causes for the delayed atmospheric response to El Niño. *J. Climate*, **16**, 1391–1403, [https://doi.org/10.1175/1520-0442\(2003\)16<1391:TNACFT>2.0.CO;2](https://doi.org/10.1175/1520-0442(2003)16<1391:TNACFT>2.0.CO;2).
- Landman, W. A., S. J. Mason, P. D. Tyson, and W. J. Tennant, 2001: Retro-active skill of multi-tiered forecasts of summer rainfall over southern Africa. *Int. J. Climatol.*, **21**, 1–19, <https://doi.org/10.1002/joc.592>.
- L'Heureux, M. L., and D. W. J. Thompson, 2006: Observed relationship between the El Niño–Southern Oscillation and the extratropical zonal-mean circulation. *J. Climate*, **2**, 276–287, <https://doi.org/10.1175/JCLI3617.1>.
- Lucas, C., B. Timbal, and H. Nguyen, 2014: The expanding tropics: A critical assessment of the observational and modeling studies. *Wiley Interdiscip. Rev.: Climate Change*, **5**, 89–112, <https://doi.org/10.1002/wcc.251>.
- Mahlalela, P. T., R. C. Blamey, and C. J. C. Reason, 2019: Mechanisms behind early winter rainfall variability in the southwestern Cape, South Africa. *Climate Dyn.*, **53**, 21–39, <https://doi.org/10.1007/s00382-018-4571-y>.
- Merryfield, W. J., and Coauthors, 2013: The Canadian seasonal to interannual prediction system. Part I: Models and initialization. *Mon. Wea. Rev.*, **141**, 2910–2945, <https://doi.org/10.1175/MWR-D-12-00216.1>.
- Mulenga, H. M., M. Rouault, and C. J. C. Reason, 2003: Dry summers over northeastern South Africa and associated circulation anomalies. *Climate Res.*, **25**, 29–41, <https://doi.org/10.3354/cr025029>.
- Philippon, N., M. Rouault, Y. Richard, and A. Favre, 2012: The influence of ENSO on winter rainfall in South Africa. *Int. J. Climatol.*, **32**, 2333–2347, <https://doi.org/10.1002/joc.3403>.
- Pohl, B., N. Fauchereau, C. J. C. Reason, and M. Rouault, 2010: Relationships between the Antarctic Oscillation, the Madden–Julian oscillation, and ENSO, and consequences for rainfall analysis. *J. Climate*, **23**, 238–254, <https://doi.org/10.1175/2009JCLI2443.1>.
- Reason, C. J. C., and D. Jagadheesha, 2005: A model investigation of recent ENSO impacts over southern Africa. *Meteor. Atmos. Phys.*, **89**, 181–205, <https://doi.org/10.1007/s00703-005-0128-9>.
- , and M. Rouault, 2005: Links between the Antarctic Oscillation and winter rainfall over western South Africa. *Geophys. Res. Lett.*, **32**, L07705, <https://doi.org/10.1029/2005GL022419>.
- , —, J.-L. Melice, and D. Jagadheesha, 2002: Interannual winter rainfall variability in SW South Africa and large scale ocean–atmosphere interactions. *Meteor. Atmos. Phys.*, **80**, 19–29, <https://doi.org/10.1007/s007030200011>.
- Ropelewski, C. F., and M. S. Halpert, 1987: Global and regional scale precipitation patterns associated with the El Niño/Southern Oscillation. *Mon. Wea. Rev.*, **115**, 1606–1626, [https://doi.org/10.1175/1520-0493\(1987\)115<1606:GARSPP>2.0.CO;2](https://doi.org/10.1175/1520-0493(1987)115<1606:GARSPP>2.0.CO;2).
- Rouault, M., B. Pohl, and P. Penven, 2010: Coastal oceanic climate change and variability from 1982 to 2009 around South Africa. *Afr. J. Mar. Sci.*, **32**, 237–246, <https://doi.org/10.2989/1814232X.2010.501563>.
- Saha, S., and Coauthors, 2014: The NCEP Climate Forecast System version 2. *J. Climate*, **27**, 2185–2208, <https://doi.org/10.1175/JCLI-D-12-00823.1>.
- Saji, N. H., B. N. Goswami, P. N. Vinayachandran, and T. Yamagata, 1999: A dipole mode in the tropical Indian Ocean. *Nature*, **401**, 360–363, <https://doi.org/10.1038/43854>.
- Scaife, A. A., and D. Smith, 2018: A signal-to-noise paradox in climate science. *npj Climate Atmos. Sci.*, **1**, 28, <https://doi.org/10.1038/s41612-018-0038-4>.
- Seager, R., N. Harnik, Y. Kushnir, W. Robinson, and J. Miller, 2003: Mechanisms of hemispherically symmetric climate variability. *J. Climate*, **16**, 2960–2978, [https://doi.org/10.1175/1520-0442\(2003\)016<2960:MOHSCV>2.0.CO;2](https://doi.org/10.1175/1520-0442(2003)016<2960:MOHSCV>2.0.CO;2).
- , T. J. Osborn, Y. Kushnir, I. R. Simpson, J. Nakamura, and H. Liu, 2019: Climate variability and change of Mediterranean-type climates. *J. Climate*, **32**, 2887–2915, <https://doi.org/10.1175/JCLI-D-18-0472.1>.
- Seidel, D. J., Q. Fu, W. J. Randel, and T. J. Reichler, 2008: Widening of the tropical belt in a changing climate. *Nat. Geosci.*, **1**, 21–24, <https://doi.org/10.1038/ngeo.2007.38>.
- Sousa, P. M., R. C. Blamey, C. J. C. Reason, A. M. Ramos, and R. M. Trigo, 2018: The ‘day zero’ Cape Town drought and the poleward migration of moisture corridors. *Environ. Res. Lett.*, **13**, 124025, <https://doi.org/10.1088/1748-9326/aaebc7>.
- Thompson, D. W. J., and J. M. Wallace, 2000: Annular modes in the extratropical circulation. Part I: Month-to-month variability. *J. Climate*, **13**, 1000–1016, [https://doi.org/10.1175/1520-0442\(2000\)013<1000:AMITEC>2.0.CO;2](https://doi.org/10.1175/1520-0442(2000)013<1000:AMITEC>2.0.CO;2).
- Tyson, P. D., and R. A. Preston-Whyte, 2000: *The Weather and Climate of Southern Africa*. 2nd ed. Oxford University Press, 396 pp.
- Vecchi, G. A., and Coauthors, 2014: On the seasonal forecasting of regional tropical cyclone activity. *J. Climate*, **27**, 7994–8016, <https://doi.org/10.1175/JCLI-D-14-00158.1>.
- Vernieres, G., M. Rienecker, R. Kovach, and C. Kepenne, 2012: The GEOS-ODAS, description and evaluation. Vol. 30, NASA Tech. Rep. NASA/TM-2012-104606, 73 pp., <https://ntrs.nasa.gov/api/citations/20140011278/downloads/20140011278.pdf>.
- Xie, P., and P. A. Arkin, 1997: Global precipitation: A 17-year monthly analysis based on gauge observations, satellite estimates, and numerical model outputs. *Bull. Amer. Meteor. Soc.*, **78**, 2539–2558, [https://doi.org/10.1175/1520-0477\(1997\)078<2539:GPAYMA>2.0.CO;2](https://doi.org/10.1175/1520-0477(1997)078<2539:GPAYMA>2.0.CO;2).